Method for bandgap interpolation of perovskite's spectral complex refractive index

Blom, Youri; Vogt, Malte Ruben; Isabella, Olindo

DOI
10.1364/OE.509982

Publication date
2024

Document Version
Final published version

Published in
Optics Express

Research Article Vol. 32, No. 3 / 29 Jan 2024 / Optics Express 4365
Optics EXPRESS

Method for bandgap interpolation of perovskite's spectral complex refractive index

YOURI BLOM,* MALTE RUBEN VOGT, OLINDO ISABELLA, AND RUDI SANTBERGEN

Delft University of Technology, Photovoltaic Materials and Devices group, Mekelweg 4, 2628 CD Delft, The Netherlands
*y.blom@tudelft.nl

Abstract: Lead halide perovskites are a promising class of materials for solar cell applications. The perovskite bandgap depends on the material composition and is highly tunable. Opto-electrical device modelling is commonly used to find the optimum perovskite bandgap that maximizes device efficiency or energy yield, either in single junction or multi-junction configuration. The first step in this calculation is the optical modelling of the spectral absorptance. This requires as input the perovskite's complex refractive index N as a function of wavelength λ. The complex refractive index consists of real part $n(\lambda)$ and imaginary part $k(\lambda)$. For the most commonly used perovskites, n and k curves are available from spectroscopic ellipsometry measurements, but usually only for a few discrete bandgap energies. For solar cell optimization, these curves are required for a continuous range of bandgap energies. We introduce new methods for generating the n and k curves for an arbitrary bandgap, based on interpolating measured complex refractive index data. First, different dispersion models (Cody-Lorentz, Ullrich-Lorentz and Forouhi-Bloomer) are used to fit the measured data. Then, a linear regression is applied to the fit parameters with respect to the bandgap energy. From the interpolated parameters, the refractive index curve of perovskite with any desired bandgap energy is finally reconstructed. To validate our method, we compare our results with methods from literature and then use it to simulate the absorptance of a single junction perovskite and a perovskite/silicon tandem cell. This shows that our method based on the Forouhi-Bloomer model is more accurate than existing methods in predicting the complex refractive index of perovskite for arbitrary bandgaps.

1. Introduction

Lead halide perovskites have become a promising class of material for solar cell applications [1–3]. One of the advantages of these perovskites is that their bandgap can be tuned by changing material composition [4,5]. This has enabled fabrication perovskite-based single junction cells with >25% efficiency and various perovskite/silicon tandem architectures with >30% efficiency, the latter being well beyond the limits of conventional single-junction silicon-based solar cells [4,5]. To find the optimal perovskite bandgap for a given multi-junction architecture, in-depth opto-electrical modelling is needed [6,7]. This requires as input the wavelength-dependent complex refractive index of each of the materials used in the cell [7]. This optical property is denoted as $N(\lambda) = n(\lambda) + i \cdot k(\lambda)$, where n is the refractive index, i is the imaginary unit, k is the extinction coefficient and λ is the wavelength. One approach for obtaining $n(\lambda)$ and $k(\lambda)$, would be to produce perovskite samples with different bandgap energies and measure the corresponding $n(\lambda)$ and $k(\lambda)$, e.g., using spectral ellipsometry or spectrophotometry [8,9]. However, this would be very time consuming as it requires a sample for each desired bandgap energy. Additionally, it requires both fabrication and measurement equipment to produce and measure all perovskite samples. A more convenient solution would be to measure $n(\lambda)$ and $k(\lambda)$ of one low-bandgap

#509982 https://doi.org/10.1364/OE.509982
Journal © 2024 Received 23 Oct 2023; revised 9 Jan 2024; accepted 11 Jan 2024; published 25 Jan 2024

Optics EXPRESS

and one high-bandgap sample and based on this reference data generate the $n(\lambda)$ and $k(\lambda)$ for any intermediate bandgap material.

In literature, different methods are presented to calculate $n(\lambda)$ and $k(\lambda)$ of perovskite with different bandgap energies by adjusting measured $n(\lambda)$ and $k(\lambda)$ reference data. The first method described by S. Albrecht et al. [10] uses the following equation to simply blueshift $n(\lambda)$ and $k(\lambda)$,

$$\lambda_{new} = \lambda - \Delta\lambda_{bg}, \tag{1}$$

where $\Delta\lambda_{bg}$ is the difference in bandgap energy between the reference data and the desired wider-bandgap energy. This method will be referred to as the "Shift" method. Another method, described by S. Manzoor et al. [11], uses the following wavelength transformation

$$\lambda_{new} = \lambda - \left(\Delta\lambda_{bg} + 10\right) \cdot \frac{\lambda}{1200}, \tag{2}$$

where $\Delta\lambda_{bg}$ is the again the difference in bandgap energy, 10 is an empirically determined offset, and 1200' refers to maximum wavelength in the region of interest [11]. This method is extended by Raja et al. to model the effect of temperature on the complex refractive index [12]. Besides just shifting, such a method also scales the data and will therefore be referred to as the "Scale" method.

These methods allow us to predict the complex refractive index for different bandgap energies by adjusting the wavelengths. The advantage of these methods is that only the refractive index for one bandgap energy is needed. However, the visible trend in the complex refractive index for different bandgap energies is more complex than a simple wavelength transformation, since also the height of the various peaks changes, as shown in Fig. 1(A). Being N the input for modeling absorptance, it is essential to calculate $n(\lambda)$ and $k(\lambda)$ accurately.

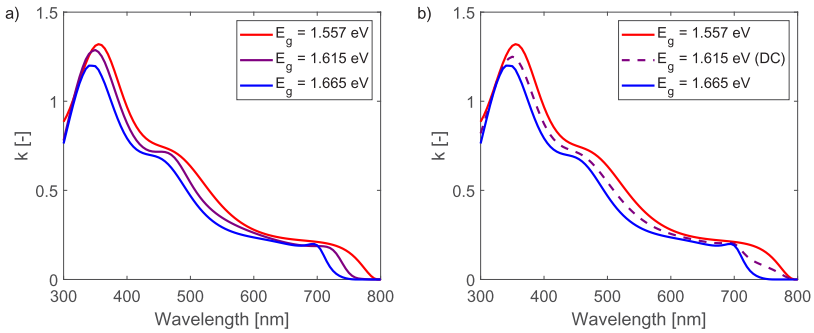

Fig. 1. (a) Measured $k(\lambda)$ of perovskite films exhibiting different bandgap energies (reproduced from [11]). (b) The DC method is applied to the middle bandgap energy to predict $k(\lambda)$.

Another approach, used by Gota, et al. [13] is to interpolate the refractive index for perovskite samples with different bandgap energies. This requires the measured $N(\lambda)$ for at least two samples, such that it can be interpolated for bandgap energies in-between. To make sure that $n(\lambda)$ and $k(\lambda)$ are still Kramers-Kronig (KK) consistent [14], the interpolation can only be applied to k, and n can be obtained via a numerical KK-integration [15]. This method will be referred to as the "Direct Interpolation" ("DC") method. Figure 1(B) shows the $k(\lambda)$ when this method is applied to the middle bandgap energy. It can be seen this leads to a more gradual slope in the region 700-800 nm, which is not typical for perovskite. Therefore, we propose a new method that accounts for the complex trends in $n(\lambda)$ and $k(\lambda)$ with varying bandgap energy, while still keeping the typical sharp cut-off for the k close to the bandgap energy.

Optics EXPRESS

2. Methodology

Our method is based on interpolating the parameters of dispersion models, that describe the absorption of the perovskite [16]. These perovskite samples should have the same composition and vary only in stoichiometry, and the corresponding bandgap energies should be known. Care should be taken when the measured $n(\lambda)$ and $k(\lambda)$ are taken from literature, as the deposition of perovskite can vary significantly.

First, as will be explained below, the complex refractive index of each material is fitted with the different dispersion models, such that the complex refractive index curve is accurately parameterized. Then, the value of the fitting parameters are interpolated such that new n and k data can be generated. We use three dispersion models, the Cody-Lorentz, Ullrich-Lorentz, and Forouhi-Bloomer model, to fit and interpolate n and k. Each dispersion model will be discussed quickly.

2.1. Cody-Lorentz model

The Cody-Lorentz (CL) model is an extension of the Tauc-Lorentz (TL) model [16–18]. In the TL model, the absorption has a quadratic dependence on the photon energy, but it does not include Urbach tails [19,20]. The CL model includes Urbach tail by defining a piece-wise function [17] for the complex part of the electric permittivity (ϵ_2) as function of energy (E). The function is split into a part describing an Urbach tail with an exponential decay, and a part written as the sum of different oscillators, fully written as

$$\epsilon_2(E) = \begin{cases} \frac{E_1}{E} \cdot e^{\frac{E-E_t}{E_U}} & 0<E \leq E_t \\ \frac{(E-E_g)^2}{E^2} \cdot \sum_{i=1}^{N_{\text{osc}}} \frac{S_i \cdot B_i \cdot E}{(E^2-E_{c,i}^2)^2+B^2 \cdot E^2} & E>E_t, \end{cases} \tag{3}$$

where E_t is the transition energy, E_u is the Urbach energy, E_1 is a parameter to guarantee continuity of ϵ_2, N_{osc} is the number of oscillators, and S_i, B_i and $E_{c,i}$ are the strength, width, and position of each oscillator. The real part of the electric permittivity (ϵ_1) can be calculated by performing a KK integration. n and k can then be obtained via the relation $(n + i \cdot k)^2 = \epsilon_1 + i \cdot \epsilon_2$.

2.2. Ullrich-Lorentz model

There are two main drawbacks for the CL model: (i) it has a discontinuous first derivative at $E = E_t$, and (ii) its quadratic dependence excludes direct semiconductor behaviour [16]. The Ullrich-Lorentz (UL) model overcomes these problems by multiplying the oscillator equation with Ullrich's continuous dielectric function [16,21,22]. The UL model expresses ϵ_2 as

$$\epsilon_2(E) = = \begin{cases} \sum_{i=1}^{N_{\text{osc}}} \frac{1}{E} \frac{S_i \cdot B_i}{(E^2-E_{c,i}^2)^2+B^2 \cdot E^2} \cdot \sqrt{E-E_g} & E \geq E_g + \frac{1}{2\beta} \\ \sum_{i=1}^{N_{\text{osc}}} \frac{1}{E \cdot \sqrt{2\beta}} \frac{S_i \cdot B_i}{(E^2-E_{c,i}^2)^2+B^2 \cdot E^2} \cdot e^{\beta(E-E_g)} & E<E_g + \frac{1}{2\beta}, \end{cases} \tag{4}$$

where β is the Urbach slope. The n and k can be obtained via the same procedure as the CL model.

2.3. Forouhi-Bloomer model

The last dispersion model we consider in this work is the Forouhi-Bloomer (FB) model [23] that directly describes k as a summation of different oscillators

$$k(E) = = \begin{cases} \sum_{i=1}^{N_{\text{osc}}} \frac{S_i \cdot (E-E_{\text{min}})^2}{\left(E-E_{c,i}\right)^2+B_i^2} & E>E_{\text{min}} \\ 0 & E \leq E_{\text{min}}, \end{cases} \tag{5}$$

Optics EXPRESS

In these equations, E_{min} corresponds to the minimum photon energy that is absorbed by the material, which is typically very similar to its bandgap energy. n can be obtained via a numerical KK integration.

It should be realized that the FB model was originally designed for amorphous materials, not for crystalline materials [23]. Additionally, it is argued that the Forouhi-Bloomer is physically inconsistent [16,18,24], as Eq. (5), does not converge to 0 as $E \rightarrow \infty$, and it does not contain time reversal symmetry, which is a fundamental condition of the classical theory of dispersion [18]. This is also acknowledged by Forouhi and Bloomer, and they have updated their model to account for these issues [24].

However, P. Löper et al. [9] showed that the original FB model can be used to fit n and k of perovskite accurately. Additionally, we show in the Supporting Information that, in the wavelength range of interest, the original FB model provides a better fit for the complex refractive index of the perovskite samples than the updated FB model. The reason for this, is that the original equations can better describe the sharp cut-off in the k close to the bandgap energy than the updated equations. We speculate this is because of the direct band gap nature of perovskite films, which mostly cease to absorb light for $E<E_g$, where the updated FB model accounts for the probability of quantum constituents such as phonon interactions [24].

2.4. Interpolating the parameter

After the data has been fitted to the dispersion model, a linear fit for all parameters is applied with respect to the bandgap energy. The refractive index curve at any desired bandgap energy can then be reconstructed from the dispersion model parameters interpolated at the desired bandgap energy. Note, that the desired bandgap energy should be in between the minimum and maximum bandgap energy of the measured samples, as it otherwise would lead to extrapolation. Although extrapolation is possible with our method, it could reduce the accuracy of the prediction. The corresponding methods will be denoted with CL^+, UL^+, and FB^+ for the different dispersion models.

3. Results

We apply the described models to three data sets with different perovskite compositions, where the stoichiometry was varied to vary the bandgap energy. The three different datasets are summarized in Table 1. The complex refractive index, the fitting of all curves, and the values for the fitting parameters can be found in the Supporting Information. These datasets are used to analyze and compare the accuracy of the described models with other models discussed in the introduction when predicting the complex refractive index, and the absorptance in a perovskite single junction and perovskite/silicon tandem cell. The numerical data of all measurements and simulations can be found in Data File 1, Data File 2, and Data File 3.

Table 1. Measured complex refractive index datasets used to validate our model

Data set	Material	Number of samples	Range of bandgap energies [eV]	Source
1	CsBr and MAPI	3	1.56 -1.67	S. Manzoor, *et al.* [11]
2	CsFAPbIBr	6	1.62 -1.80	J. Werner, *et al.* [25]
3	FAI, FABR, and MACI	5	1.58 -1.77	W. Raja, *et al.* [12]

3.1. Predicting the complex refractive index

To analyze the accuracy of our method, we divide each set of measured data into two parts: i) fitting data, and ii) validation data. We illustrate this procedure using dataset 2, which covers

Optics EXPRESS

bandgap energies ranging from 1.62 eV to 1.80 eV. The sample with a bandgap energy of 1.67 eV is used as validation data, and the remaining samples are used as fitting data. The $n(\lambda)$ and $k(\lambda)$ are then reconstructed for a bandgap energy of 1.67 eV and compared with the validation data.

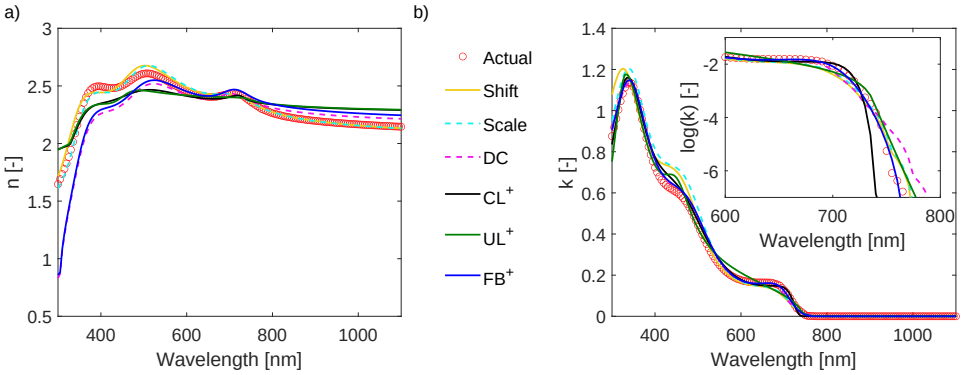

Fig. 2. Comparison of the actual (a) $n(\lambda)$ and (b) $k(\lambda)$ dataset of a perovskite sample exhibiting $E_g = 1.67$ eV compared with different methods. The inset diagram in (b) zooms in the wavelength range 600-800 nm for better appreciating the performance of the developed methods compared to the reference methods. The sample is taken from dataset 2.

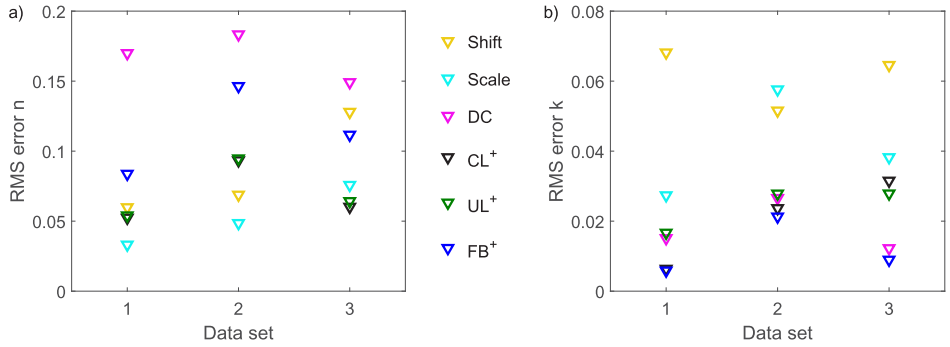

Fig. 3. The RMS error for (a) $n(\lambda)$ and (b) $k(\lambda)$ curves when predicting them with different methods. The FB$^+$ method shows more than 55% lower error for $k(\lambda)$ in all datasets, whereas it has a similar error for $n(\lambda)$ compared to the other methods.

Figure 2 shows that especially the FB$^+$ method tends to have a better fit with the measured validation data. This is repeated for all samples in the dataset, excluding the samples with the smallest and largest bandgap energy in the data set. All data sets can be found in the Supporting Information. To quantify the quality of the prediction, we use the Root-Mean-Square (RMS) of the spectral deviation between the measured and reconstructed $n(\lambda)$ and $k(\lambda)$ data. Figure 3 compares the average RMS error in the n and k data for all datasets between the different methods. The FB$^+$, CL$^+$, UL$^+$ methods have similar accuracy for predicting the n-data, compared to the other methods. However, these method gives more accurate k-data for all datasets compared to the Shift and Scale method.

3.2. *Predicting the absorptance of a single junction perovskite cell*

It should be realized that $n(\lambda)$ and $k(\lambda)$ data of (semiconductor) materials are used as input to calculate the absorptance in layers comprised in a solar cell. Therefore, we analyze the

Optics EXPRESS

accuracy of the developed methods by simulating the absorptance in a single-junction perovskite solar cell and a perovskite/silicon double-junction solar cell (also known as tandem device) by using both the actual and the predicted complex refractive index of the perovskite absorber layer. The simulations are done with the software GenPro4 [26]. The structure of the simulated single-junction perovskite cell can be found in Fig. 4(A) and is based on the top cell of the perovskite/silicon tandem cell presented by Al-Ashouri et al. [27]. Our methods will be compared with the other methods from literature, similar to the previous comparison. An example of the simulated absorptance based on refractive index data input from the different methods and the simulated cell is shown in Fig. 4. The simulated absorptance for all perovskite samples and predictions can be found in the supporting information.

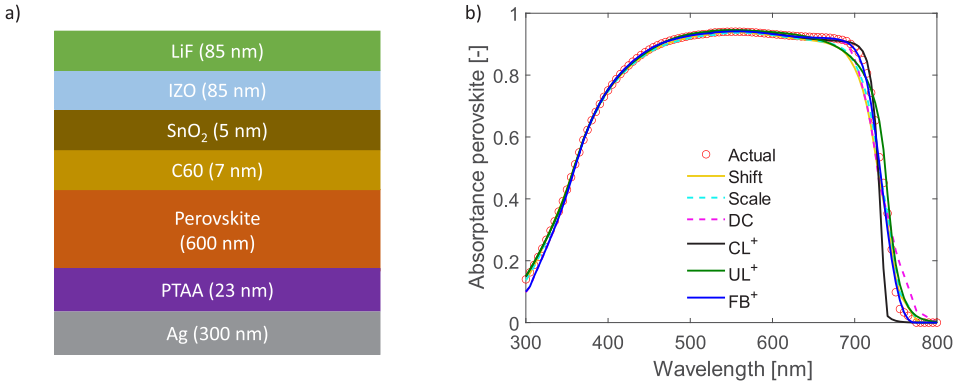

Fig. 4. (a) Optical system describing the simulated single-junction perovskite solar cell. (b) Absorptance of the perovskite layer as simulated with measured complex refractive index (red circles, taken from dataset 2 [25]), or computed complex refractive index via the different methods. The considered solar cell comprises a perovskite absorber layer E_g= 1.67 eV.

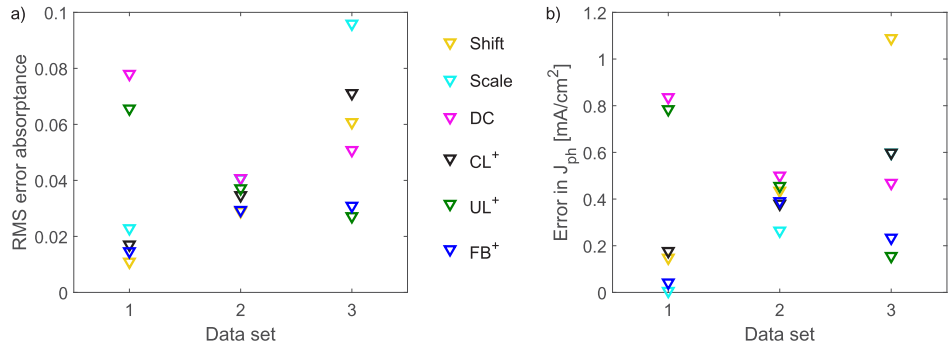

Fig. 5. (a) RMS error in absorptance of perovskite and (b) error in J_{ph} of perovskite single junction cell simulated with $n(\lambda)$ and $k(\lambda)$ data of perovskite absorber generated using different methods.

Deviations mainly occur in the wavelength range 650-750 nm. This comes from the fact that the absorption depends on the product $\alpha \cdot d$ (where $\alpha = \frac{4\pi \cdot k}{\lambda}$, and d is the thickness). If $\alpha \cdot d >> 1$, light is fully absorbed, and if $\alpha \cdot d << 1$, light is fully transmitted regardless of the exact value of alpha. This means that an error in $k(\lambda)$ has most impact on the absorptance when $\alpha \cdot d$ is around

Optics EXPRESS

1. This is the case when

$$\alpha \cdot d = \frac{4\pi \cdot k}{\lambda} \approx 1 \tag{6}$$

$$k \approx \frac{\lambda}{4\pi \cdot d}. \tag{7}$$

As λ and d have the same order of magnitude, it is most important to model k accurately when $k \approx \frac{1}{4\pi} \approx 0.08$. As can be seen in Fig. 2, this is the wavelength range of 650-750 nm. Besides this range, there are also deviations in the wavelength range 750-800 nm. This can be explained by looking at the inset in Fig. 2(b), where it shows that especially the DC method overestimates the k in this region. On the contrary, the CL^+ underestimates $k(\lambda)$, as shown in inset of Fig. 2(B), leading to an underestimation of the absorptance. Similar to the previous comparison, we will use the RMS error of the spectral absorptance of the perovskite layer to compare our developed methods with the methods from literature. Additionally, the deviation of the implied photocurrent density (J_{ph}) of each method is calculated compared to the reference sample. The RMS error and J_{ph}-deviation of every curve is calculated and the average for each data set is shown in Fig. 5. The FB^+ method yields an error in the absorptance of the perovskite layer of maximum 0.03 for all datasets, which is smaller compared to the other methods. This can be explained by the fact that this method has a smaller error in the $k(\lambda)$ spectrum, especially in the critical wavelength region of 650-750 nm. Although this method has the lowest error in the absorptance, it does not always shows the smallest deviation in photo-generated current. However, if a method underestimates the absorptance in a specific wavelength region, and overestimates the absorptance in a different wavelength region, the errors can compensate each other, reducing the deviation in the implied photocurrent. This can explain why the "Scale" method has a smaller error in J_{ph}, but a larger RMS error for the absorptance. Therefore, the error in the absorptance should be used as the key metric to quantify the accuracy.

3.3. Predicting the absorptance of a perovskite/silicon tandem cell

The structure of the optically simulated perovskite/silicon tandem device is also taken from [27] and reproduced in Fig. 6(A). Like in the case of single-junction perovskite solar cell, we simulate the optical situation in this tandem cell as function of the actual and predicted complex refractive index of the perovskite layer. In Fig. 6(B) and 6(C) we report the comparison of the absorptances of perovskite and silicon, respectively. Also in this case, deviations in both absorptances mainly occur in the wavelength range of 650-750 nm for the reasons explained before.

The average absorptance RMS error and J_{ph}-deviation are reported in Fig. 7, where the FB^+ method shows the smallest RMS error for the perovskite absorptance and, in most cases, also the smallest RMS error for the silicon absorptance. However, this does not always translate into the smallest deviation in photo-generated current density for the abovementioned over/ underestimation in different wavelength regions. Therefore, also for the double-junction perovskite/silicon solar cell, we confirm the accuracy of the absorptance should be used as the main characteristic to compare different methods.

3.4. Overview of the different metrics

Table 2 presents the average values of the metrics for the different methods. Interestingly, the DC, CL^+, and UL^+, method have a relative high accuracy for the prediction of n and k, but have a low accuracy for the prediction of the absorption. This can be understood by the fact that it is important to accurately predict the k in the critical wavelength region of 650-750 nm, as this mostly dominates the error in the EQE. With the exception of n, the FB^+ provides the highest accuracy for all metrics, as this method provides a high accuracy for the critical wavelength region. Therefore, we argue that using the FB^+ model is most accurate in predicting the complex refractive index of perovskite.

Optics EXPRESS

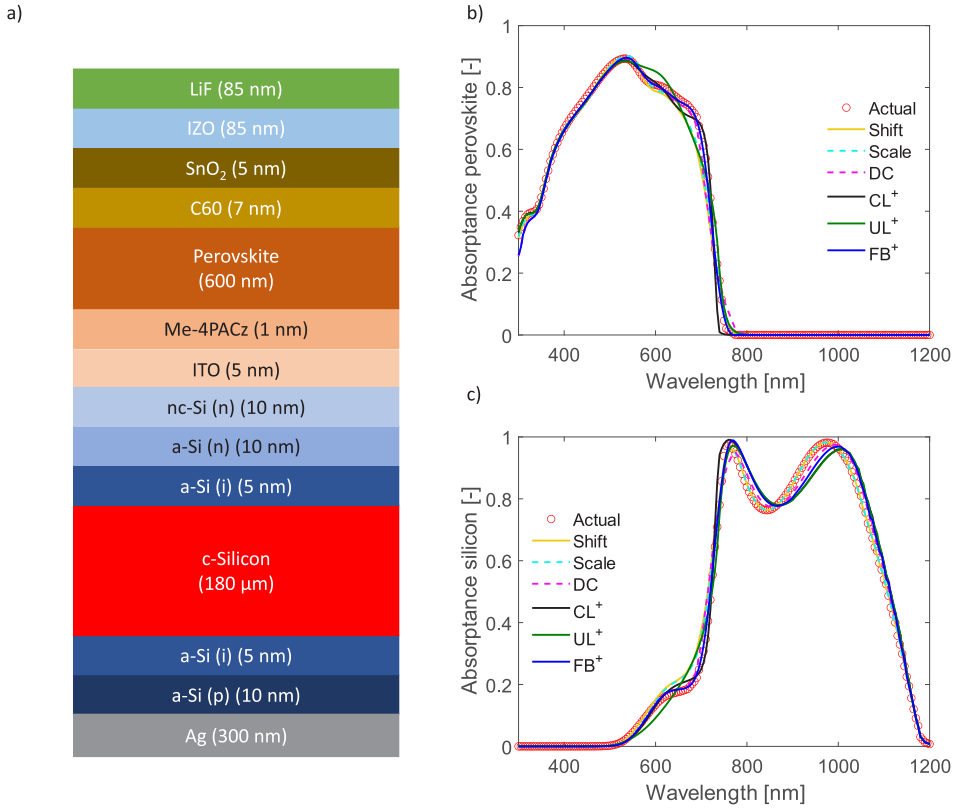

Fig. 6. (a) Optical system describing the simulated double-junction perovskite/silicon solar cell. (b) and (c) Absorptance of the perovskite and silicon absorbers, respectively, as simulated with measured complex refractive index (red circles) of perovskite absorber layer exhibiting E_g = 1.67 eV (taken from dataset 2 [25]) or computed complex refractive index via the different methods.

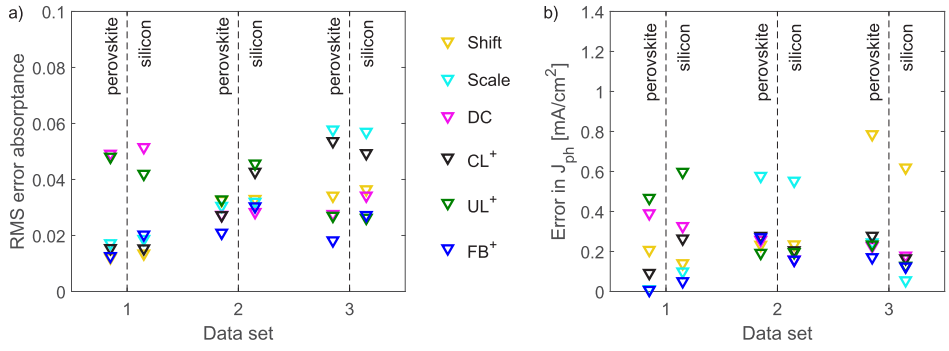

Fig. 7. (a) RMS error in absorptance of perovskite or silicon and (b) error in J_{ph} of perovskite or silicon simulated with $n(\lambda)$ and $k(\lambda)$ data of perovskite absorber, generated using different methods.

Optics EXPRESS

Table 2. An overview of the different metrics to evaluate the accuracy of the methods. For each metric, the average values over the different datasets are taken. The FB^+ model has the lowest error for the *k* and all EQE's

	RMS error				
	Refractive index		Absorptance		
Method	n	k	Perovskite (single junction)	Perovskite (top cell)	Silicon (bottom cell)
Shift	0.086	0.061	0.034	0.026	0.028
Scale	0.053	0.041	0.029	0.035	0.036
DC	0.17	0.018	0.057	0.035	0.038
CL^+	0.069	0.021	0.041	0.032	0.036
UL^+	0.071	0.024	0.043	0.036	0.038
FB^+	0.11	0.012	0.025	0.017	0.026

Figure 8 shows the result of applying the FB^+ to predict $k(\lambda)$ for different bandgap energies. In contrast to the DC method, shown in Fig. 1(B), the predictive curves maintain their sharp cut-off, but also follow the visible trends.

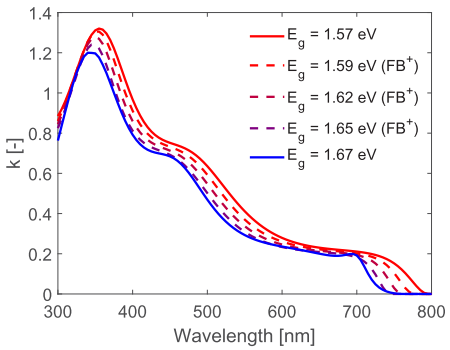

Fig. 8. The result of using the FB^+ to interpolate k for different bandgap energies. In contrast with the DC method (Fig. 1(B), the predicted curves maintain their sharp cut-off.

4. Conclusion

In conclusion, our work introduces new methods for interpolating the complex refractive index of novel perovskite materials. This enables us to model the optical performance of perovskite layers with diverse bandgap energies without the need of fabricating and measuring the optical properties of such samples. This can reduce the cost and additionally speed up the development process of perovskite-based solar cells and other devices. Our method is based on different dispersion models, that are used to fit the complex refractive index of all samples within a dataset. Then, for all parameters, a linear fit is applied with respect to the bandgap energy, such that the complex refractive index of a perovskite with the desired bandgap energy can be generated. The method based on the Forouhi-Bloomer model shows the best accuracy in predicting the absorptance and the implied photocurrent density of both single-junction perovskite solar cells and perovskite/silicon double-junction solar cell. In fact, this method has a significantly lower error for the $k(\lambda)$ data, while demonstrating a similar error for the $n(\lambda)$ data to the other methods.

Semiconductor device modelling and energy yield simulations of perovskite-based solar cells and modules benefit from better accuracy and freedom in selection of bandgaps as they require optical simulation as an input. Therefore, our method will play a key role in optimizing energy

Optics EXPRESS

yield of perovskite-based solar devices by adjusting the bandgaps to the different outdoor spectral irradiation conditions around the world. As a consequence, this might enable a new era for location optimized PV modules.

Disclosures. The authors declare no conflicts of interest.

Data availability. Data underlying the results presented in this paper are available in the Data File 1 [28], Data File 2 [29], and Data File 3 [30].

Supplemental document. See Supplement 1 for supporting content.

References

1. Y. Zhang and N.-G. Park, "Quasi-Two-Dimensional Perovskite Solar Cells with Efficiency Exceeding 22%," ACS Energy Lett. **7**(2), 757–765 (2022).
2. Y. Tong, A. Najar, L. Wang, *et al.*, "Wide-bandgap organic–inorganic lead halide perovskite solar cells," Adv. Sci. **9**(14), 2105085 (2022).
3. K. Sakhatskyi, R. A. John, A. Guerrero, *et al.*, "Assessing the Drawbacks and Benefits of Ion Migration in Lead Halide Perovskites," ACS Energy Lett. **7**(10), 3401–3414 (2022).
4. R. Sharma, A. Sharma, S. Agarwal, *et al.*, "Stability and efficiency issues, solutions and advancements in perovskite solar cells: A review," Sol. Energy **244**, 516–535 (2022).
5. S. Akhil, S. Akash, A. Pasha, *et al.*, "Review on perovskite silicon tandem solar cells: Status and prospects 2T, 3T and 4T for real world conditions," Mater. & Des. **211**, 110138 (2021).
6. Š. Tomšič, M. Jošt, K. Brecl, *et al.*, "Energy yield modeling for optimization and analysis of perovskite-silicon tandem solar cells under realistic outdoor conditions," Adv. Theory Simulations **6**(4), 2200931 (2023).
7. M. T. Hörantner and H. J. Snaith, "Predicting and optimising the energy yield of perovskite-on-silicon tandem solar cells under real world conditions," Energy & Environ. Sci. **10**(9), 1983–1993 (2017).
8. A. Tejada, S. Braunger, L. Korte, *et al.*, "Optical characterization and bandgap engineering of flat and wrinkle-textured $FA_{0.83}Cs_{0.17}Pb(I_{1-x}Br_x)_3$ perovskite thin films," J. Appl. Phys. **123**(17), 175302 (2018).
9. P. Löper, M. Stuckelberger, B. Niesen, *et al.*, "Complex Refractive Index Spectra of $CH_3NH_3PbI_3$ Perovskite Thin Films Determined by Spectroscopic Ellipsometry and Spectrophotometry," J. Phys. Chem. Lett. **6**(1), 66–71 (2015).
10. S. Albrecht, M. Saliba, J.-P. Correa-Baena, *et al.*, "Towards optical optimization of planar monolithic perovskite/silicon-heterojunction tandem solar cells," J. Opt. **18**(6), 064012 (2016).
11. S. Manzoor, J. Häusele, K. A. Bush, *et al.*, "Optical modeling of wide-bandgap perovskite and perovskite/silicon tandem solar cells using complex refractive indices for arbitrary-bandgap perovskite absorbers," Opt. Express **26**(21), 27441 (2018).
12. W. Raja, T. G. Allen, A. A. Said, *et al.*, "Temperature-Dependent Optical Modeling of Perovskite Solar Cells," J. Phys. Chem. C **126**(33), 14366–14374 (2022).
13. F. Gota, S. X. An, H. Hu, *et al.*, "Energy Yield Modeling of Bifacial All-Perovskite Two-Terminal Tandem Photovoltaics," Adv. Opt. Mater. **11**(3), 2201691 (2023).
14. T. Dethe, H. Gill, D. Green, *et al.*, "Causality and dispersion relations," Am. J. Phys. **87**(4), 279–290 (2019).
15. K. Ohta and H. Ishida, "Comparison among several numerical integration methods for kramers-kronig transformation," Appl. Spectrosc. **42**(6), 952–957 (1988).
16. K. Lizárraga, L. A. Enrique-Morán, A. Tejada, *et al.*, "New optical dispersion models for the accurate description of the electrical permittivity in direct and indirect semiconductors," J. Phys. D: Appl. Phys. **56**(36), 365106 (2023).
17. A. S. Ferlauto, G. M. Ferreira, J. M. Pearce, *et al.*, "Analytical model for the optical functions of amorphous semiconductors from the near-infrared to ultraviolet: Applications in thin film photovoltaics," J. Appl. Phys. **92**(5), 2424–2436 (2002).
18. D. Franta, M. Čermák, J. Vohánka, *et al.*, "Dispersion models describing interband electronic transitions combining Tauc's law and Lorentz model," Thin Solid Films **631**, 12–22 (2017).
19. F. Urbach, "The Long-Wavelength Edge of Photographic Sensitivity and of the Electronic Absorption of Solids," Phys. Rev. **92**(5), 1324 (1953).
20. J. D. Dow and D. Redfield, "Toward a Unified Theory of Urbach's Rule and Exponential Absorption Edges," Phys. Rev. B **5**(2), 594–610 (1972).
21. B. Ullrich and C. Bouchenaki, "Bistable Optical Thin CdS Film Devices: All-Optical and Optoelectronic Features," Jpn. J. Appl. Phys. **30**(7B), L1285 (1991).
22. B. Ullrich, S. Yano, R. Schroeder, *et al.*, "Analysis of single- and two-photon-excited green emission spectra of thin-film cadmium sulfide," J. Appl. Phys. **93**(4), 1914–1917 (2003).
23. A. R. Forouhi and I. Bloomer, "Optical dispersion relations for amorphous semiconductors and amorphous dielectrics," Phys. Rev. B **34**(10), 7018–7026 (1986).
24. A. R. Forouhi and I. Bloomer, "New dispersion equations for insulators and semiconductors valid throughout radio-waves to extreme ultraviolet spectral range," J. Phys. Commun. **3**(3), 035022 (2019).
25. J. Werner, G. Nogay, F. Sahli, *et al.*, "Complex Refractive Indices of Cesium–Formamidinium-Based Mixed-Halide Perovskites with Optical Band Gaps from 1.5 to 1.8 eV," ACS Energy Lett. **3**(3), 742–747 (2018).

Optics EXPRESS

26. R. Santbergen, T. Meguro, T. Suezaki, *et al.*, "GenPro4 Optical Model for Solar Cell Simulation and Its Application to Multijunction Solar Cells," IEEE J. Photovoltaics **7**(3), 919–926 (2017).
27. A. Al-Ashouri, E. Köhnen, B. Li, *et al.*, "Monolithic perovskite/silicon tandem solar cell with >29% efficiency by enhanced hole extraction," Science **370**(6522), 1300–1309 (2020).
28. Y. Blom, M. R. Vogt, O. Isabella, *et al.*, "Blom interpolation nk dataset1,", figshare (2023), https://doi.org/10.6084/m9.figshare.24798507.
29. Y. Blom, M. R. Vogt, O. Isabella, *et al.*, "Blom interpolation nk dataset2," figshare (2023) https://doi.org/10.6084/m9.figshare.24798510.
30. Y. Blom, M. R. Vogt, O. Isabella, *et al.*, "Blom interpolation nk dataset3," figshare (2023), https://doi.org/10.6084/m9.figshare.24798513.